www.czasopisma.pan.pl PAN POLSKA AKADEMIA NAUK www.journals.pan.pl

Arch. Metall. Mater., Vol. 61 (2016), No 1, p. 445–450

DOI: 10.1515/amm-2016-0080

K. BŁOCH*,#

STRUCTURE AND SOFT MAGNETIC PROPERTIES OF THE AMORPHOUS ALLOYS: $Fe_{61}Co_{10}Ti_{3-X}Y_{6+X}B_{20}$ (x = 0, 1)

This paper presents studies relating to the structure, soft magnetic properties and thermal stability of the following bulk amorphous alloys: $Fe_{61}Co_{10}Ti_{3-x}Y_{6+x}B_{20}$ (x = 0, 1). On the basis of the performed X-ray diffraction studies and Mössbauer spectroscopy, it was found that investigated samples were amorphous in the as-cast state. The DSC curve obtained for $Fe_{61}Co_{10}Ti_2Y_7B_{20}$ alloy exhibited one exothermic peak, while for the $Fe_{61}Co_{10}Ti_3Y_6B_{20}$ sample, two peaks were distinguishable. The change in the chemical structure of the investigated alloys has a major effect on their soft magnetic properties; especially on coercivity and saturation magnetization. On the basis of the magnetization curves analysis, the spin wave stiffness parameter D_{sp} were determined for the investigated alloys.

1. Introduction

The first amorphous alloys, based on Fe, were made in 1967 by P. Douwez [1]. Unfortunately, the obtained samples of the Fe–P–C alloy, in the form of a ribbon, were too thin for common use. An increase in the thickness of the amorphous ribbons to greater than 120 μm led to crystallization of the alloy. For many research centres, an increase in the thickness of manufactured Fe-based amorphous alloys for the electrotechnical industry applications became the goal. The breakthrough in the manufacturing of amorphous alloys with thicknesses of greater than the limit for the ribbon samples came 30 years after Douwez obtained the first amorphous ribbon. The theory allowing repeatable production of bulk amorphous alloys has been developed.

It is worth mentioning, that the Fe-based amorphous alloys exhibit unique application parameters depending on their full chemical composition [2-6]. Particular attention should be given to bulk ferromagnetic amorphous alloys, which exhibit so-called 'soft magnetic properties' [7-10]. Due to their relatively high values of saturation magnetization and magnetic permeability, and their low values of coercivity and total losses related with de-magnetizating, these materials make an excellent basis for the fabrication of energy-efficent transformer cores. In addition, these alloys possess virtually zero magnetostriction and very low value of 'energy of effective anistropy', which means that the Fe-based amorphous alloys can be easily demagnetized, and change in their dimensions during this process is small.

In recent years, many groups of Fe-based alloys have been created [11]. These groups include Fe–Co–Ti–Y–B, created by modification of $Fe_{72}Y_xTi_yB_{22}$ alloy (where: x and y = 1, 2, 3) [12]. Introduction of Co atoms, as a replacement for 10 at% of Fe atoms, resulted in an increase in the Curie temperature, which for the original alloy was equal to 551 K. Basic research into new materials, created by manipulation of soft magnetic properties through the introduction of minor changes in chemical composition, is very important; it will improve the possibilities for their applications.

Within the volume of amorphous alloys, it is difficult to distinguish an ideal cell to describe the structure (as in the case of the crystalline materials). Therefore it is difficult to identify the structural defects in their volume. In the paper by H. Kronmüller [13], it is stated that, in the amorphous materials below the Curie temperature, all spins are parallel. However, in their volume, microareas could be found where, due to existing stress fields, the spin directions are no longer parallel through magnetoelastic interactions [14]. Above the value of the magnetic field at which the increase in magnetization is connected with the presence of structural defects, the Holstein-Primakoff paraprocess exists. This effect is related with the dumping by strong magnetic field of thermally-induced spin waves. Analysis of the initial magnetization curve in the Holstein-Primakoff paraprocess region allows the determination of a parameter describing the stiffness of the spin wave (Dsp). Parameter Dsp is described by the following equation [15]:

$$D_{sp} = \frac{1}{3} S J_{ex}(a) a^2 z_m \tag{1}$$

where:
S – the spin value in the distance from the central atom,
J_{ex} – the local exchange integral,
a – the distance to the nearest–neighbour atoms,
z_m – the number of nearest–neighbour magnetic atoms.

Dsp is connected with the changes in the nearest neighbourhood of the iron atoms.

The iron-rich amorphous materials are very good materials

* CZESTOCHOWA UNIVERSITY OF TECHNOLOGY, INSTITUTE OF PHYSICS, 19 ARMII KRAJOWEJ AV., 42-200 CZESTOCHOWA, POLAND
# Corresponding author: 23kasia1@wp.pl

for investigation using Mössbauer spectroscopy. Analysis of the distribution of the hyperfine field on the ^{57}Fe nuclei allows the extraction of information about the nearest neighbourhood of the iron atoms [15].

This paper presents the results of Mössbauer spectroscopy investigations and magnetization studies (conducted in strong magnetic fields) for the group of alloys: $Fe_{61}Co_{10}Ti_{3-x}Y_{6+1}B_{20}$ *(where: x = 0, 1).*

2. Materials and methods

The samples used in the investigations were made using high purity elements: Fe-99.99%, Co-99.98%, Ti-99.99% and Y-99.98%. The element boron was added in the form of Fe45.4B54.6 alloy. The samples were produced in the form of rods, of diameter 1 mm and length 1 cm, using a suction casting method. The structure of the alloy was investigated by means of X-ray diffractometry, using an Bruker Advance 8 X-ray diffractometer equipped with a CuKα lamp. The investigations were carried out over the 2Θ range from 30° to 120°, with a measurement step of 0.02° and 5 s exposure time per step. The microstructure of the rods was investigated using a POLON Mössbauer spectrometer featuring a 57Co radiation source with activity of 50 mCi and half-life time of 270 days. The thermal stability was investigated using differential scanning calorimeter. DSC curves were recorded at the heating rate of 10 K/min. The magnetic properties of the alloys were investigated using a LakeShore magnetometer (model 7301) with vibrating sample, working in the magnetic field range of up to 2T. All investigations of the structure, microstructure and magnetic properties were carried out at room temperature on samples that had been powdered using a low-energy process.

3. Results and discussion

Fig.1 shows X-ray diffraction patterns recorded for the investigated rod-shaped samples.

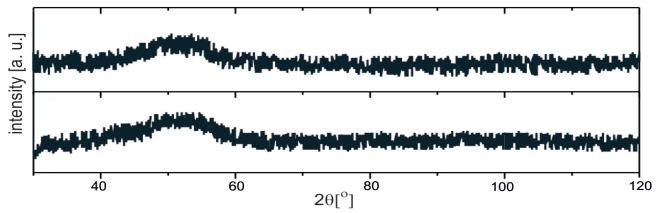

Fig. 1. X-ray diffraction patterns obtained for powdered samples in the as-quenched state: a - $Fe_{61}Co_{10}Ti_3Y_6B_{20}$, b- $Fe_{61}Co_{10}Ti_2Y_7B_{20}$

The X-ray diffraction patterns, presented in Fig. 1, each consist only of a single broad maximum, situated in the 2Θ-angle within the range from 30º to 120º. This maximum, which is also known as the 'amorphous halo', is typical for the amorphous materials.

The Mössbauer spectra, obtained from recoil free emission and absorption of gamma radiation γ, are presented in Fig. 2 a,b.

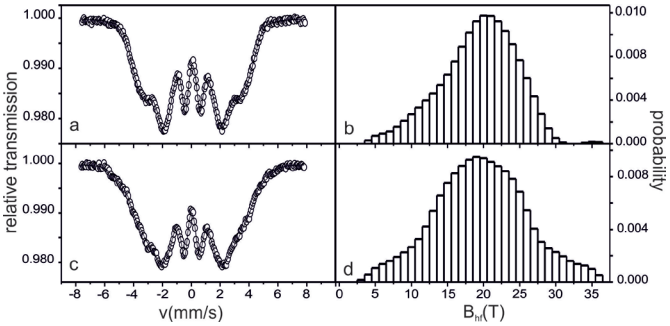

Fig. 2. Transmission Mössbauer spectra (a, b) and hyperfine field distributions of 57Fe nuclei (c, d) for the samples of: a - $Fe_{61}Co_{10}Ti_3Y_6B_{20}$, b- $Fe_{61}Co_{10}Ti_2Y_7B_{20}$

The featured Mössbauer spectra consist of asymmetrical and overlapping lines. This shape of spectrum is typical for materials with an amorphous structure [16, 17]. Numerical analysis of the recorded Mössbauer spectra facilitated the derivation of the corresponding hyperfine field distributions of ^{57}Fe nuclei.

The hyperfine field distributions calculated for the investigated samples are presented in Fig.2 c,d.

The spectra are characteristic for the amorphous ferromagnets and have a form of asymmetric sextets with broad and overlapped lines. The hyperfine magnetic field distributions $P(B_{hf})$ for investigated alloys are wide. At least two components can be distinguished, that suggest the presence of regions in the sample with different iron concentrations. The Bhf distribution obtained for the sample of $Fe_{61}Co_{10}Ti_2Y_7B_{20}$ alloy is more symmetrical, exhibiting evenly distributed high- and low-field components. Data obtained from numerical analysis of the transmission Mössbauer spectra are presented in Table 1.

On the basis of the data presented in Table 1, it can be stated that the sample of $Fe_{61}Co_{10}Ti_3Y_6B_{20}$ alloy possesses the lower value of the distribution dispersion; this means that this alloy has the simplest structure with regard to the configuration of the neighbourhoods surrounding the Fe atoms. The value of the parameter B_{hf} decreases with Y concentration because the magnetic structure becomes more non-collinear due to the exchange interaction fluctuations.

TABLE 1

Dispersion of the distribution (average standard deviation of the hyperfine field distribution) - S_D; average magnetic hyperfield - B_{hf}

Parameter Alloy composition	S_D	B_{hf} [T]
$Fe_{61}Co_{10}Ti_3Y_6B_{20}$	5.20	19.29
$Fe_{61}Co_{10}Ti_2Y_7B_{20}$	6.33	19.60

Fig. 3 presents, for all of the investigated samples, the isochronal DSC (Differential Scanning Calorimetry) curves, recorded at a heating speed of 10 K/min. In the case of the $Fe_{61}Co_{10}Ti_2Y_7B_{20}$ alloy, only one exothermic maximum can be observed. On the DCS curves for the second samples, two maxima are visible which are situated close to each other. The first maximum is related to the creation of α-FeCo crystalline grains from the nuclei, frozen during

the production process of the alloys. The second maximum is connected with the growth of crystalline grains created earlier and in the process of creating α-FeCo crystalline phase grains from embryos created during the annealing process.

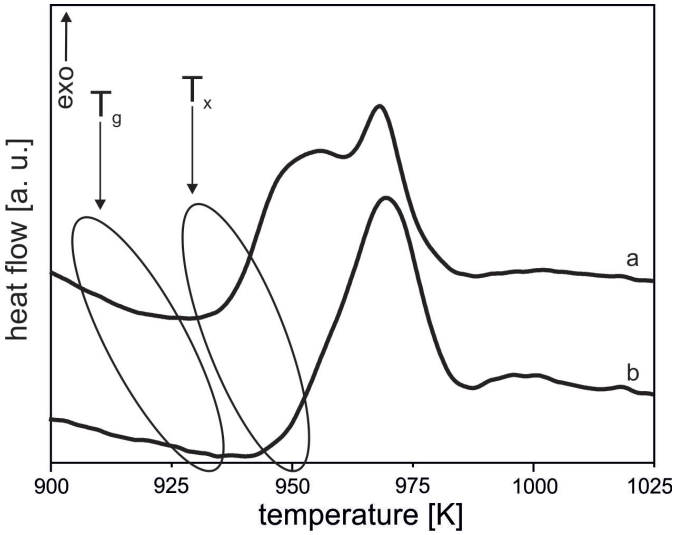

Fig. 3. The DCS curves recorded at heating speed of 10K/min. for the following bulk amorphous alloys, in the as-quenched state: $Fe_{61}Co_{10}Ti_4Y_5B_{20}$ (a), $Fe_{61}Co_{10}Ti_3Y_6B_{20}$ (b), $Fe_{61}Co_{10}Ti_2Y_7B_{20}$ (c)

On the DCS curves, the crystallization onset temperature T_x and glass transition temperature T_g have been denoted. From the curves presented in Fig. 4, it can be seen that, with an increase in Y content in the alloy, the values of T_x and T_g are being shifted towards higher temperatures. The difference between T_x and T_g is called the supercooled liquid range (ΔT_x), whose value could be an indirect measure of an alloy's glass-forming ability (GFA). In the case of most of the Fe-based alloys, the wider the value of the supercooled liquid range, the higher the GFA of the alloy. For the investigated alloys, the factor determining the value of ΔT_x is the Ti and Y content (Fig. 3). On the basis of the obtained results, it was found that subsitution of Ti atoms by Y atoms resulted in a decrease in GFA, which is in agreement with [18].

Fig. 4 shows the static magnetic hysteresis loops, measured for the investigated samples in the as-quenched state.

The static hysteresis loops, presented in Fig. 4, have a shape which is typical of that expected for soft magnetic materials [19]. From measurement of the hysteresis loops, values of saturation magnetization and coercivity have been obtained (Table 2).

TABLE 2

Data obtained from analysis of the static hysteresis loops: $\mu_0 M$ - magnetization, H_c - coercivity

Parameter / Alloy:	Ms [T]	H_c [A/m]
$Fe_{61}Co_{10}Ti_3Y_6B_{20}$	1.12	3.2
$Fe_{61}Co_{10}Ti_2Y_7B_{20}$	1.14	2.4

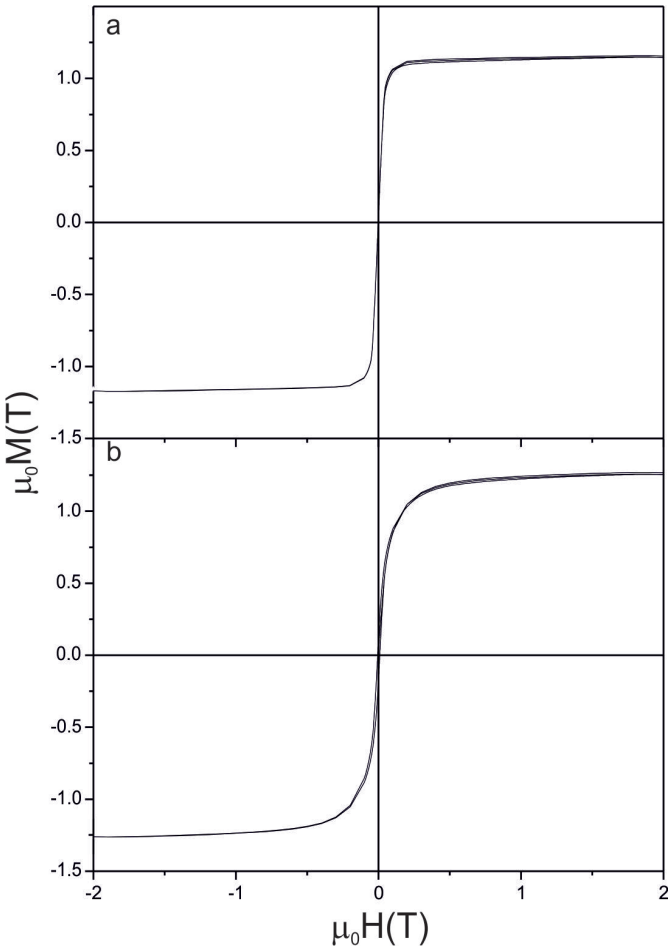

Fig. 4. The static hysteresis loops, measured for the following bulk amorphous alloys: $Fe_{61}Co_{10}Ti_3Y_6B_{20}$ (a), $Fe_{61}Co_{10}Ti_2Y_7B_{20}$ (b)

The $Fe_{61}Co_{10}Ti_2Y_7B_{20}$ alloy exhibit the higher value of saturation magnetization and lower values coercivity. The structure of this alloy can be expected to be the most relaxed, and an increase in the volume occupied by Y improves the magnetic properties of the material. In the case of the amorphous materials, the dominant mechanism in the magnetic hysteresis is the pinning of the domain wall at local stress centres during solidification of the alloy. The longer the solidification time, the more atoms are able to take their locally ordered positions. This leads to higher atomic packing density in the structure and a decrease in the 'free volumes'[20] . According to [21], an increase in the volume occupied by Y in the alloy is associated with the observation of a decrease in the number of the 'free volumes'; this, in turn, is closely connected with the quenching speed during the production process of the alloy. That is why it can be stated that the value of corecivity in each of the investigated alloys depends on the chemical composition, and is connected to changes in the free volumes.

In strong magnetic fields, as a result of the short-range stresses, the material is not homogeneously magnetized. An increase in magnetization is observed with increasing value of induction of the magnetizing field; this is due to microscopic rotation of the magnetic moment and the Holstein-Primakoff paraprocess.

The high-field magnetization curves $\mu_0 M((\mu_0 H)^{1/2})$ for the investigated alloys are presented in Fig. 5.

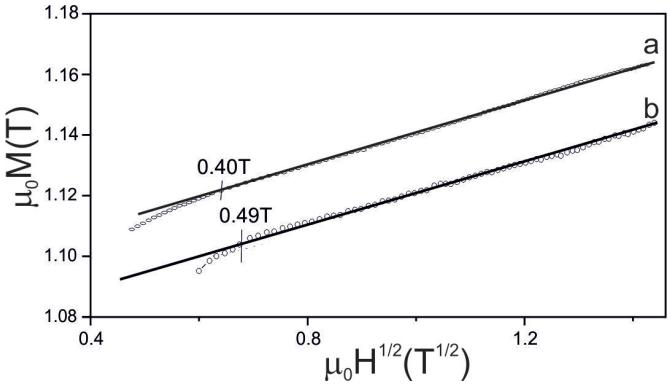

Fig. 5. The high-field magnetization curves μ0M((μ0H)1/2) measured for the following bulk amorphous alloys: $Fe_{61}Co_{10}Ti_3Y_6B_{20}$ (a), $Fe_{61}Co_{10}Ti_2Y_7B_{20}$ (b)

The linear relationships of $\mu_0M((\mu_0H)^{1/2})$, presented in Fig. 5, confirm that, above the magnetic field of 0.40 T for the $Fe_{61}Co_{10}Ti_3Y_6B_{20}$ alloy, and above 0.49 T for the $Fe_{61}Co_{10}Ti_2Y_7B_{20}$ alloy, the magnetization process is connected with dumping of the thermally-induced spin waves: the so-called Holstein-Primakoff paraprocess.

Data obtained from analysis of the high-field magnetization curves are assembled in Table 3.

TABLE 3
The experimental value of the b parameter and spin wave stiffness parameter D_{sp}

Parameter / Alloy:	b [$T^{1/2}$]	D_{sp} [10^{-2}eVnm^2]
$Fe_{61}Co_{10}Ti_3Y_6B_{20}$	0.0365	60
$Fe_{61}Co_{10}Ti_2Y_7B_{20}$	0.0350	62

The higher the value of the spin wave stiffness parameter was obtained for the $Fe_{61}Co_{10}Ti_2Y_7B_{20}$ alloy. Changes in D_{sp} are connected with the changes in the number of magnetic atoms in the nearest neighbourhood and distances between them. A higher value of the spin wave stiffness parameter indicates an increase in the number of magnetic atoms in the nearest neighbourhood, which is connected to the creation of short-range chemical ordering [15]. This is consistent with Mössbauer and magnetic investigations.

The advantageous influence, for an increase in the atomic packing density, results from having substantial differences in the atomic radii between Y (182 pm) and the other elements of this alloy, including: Fe (140 pm), Co (135 pm), Ti (140 pm) and B (87 pm). In addition, the high value of the negative mixing heat between Y and B (-35 kJ/mol), in comparison to that between Fe and B (-11 kJ/mol), could lead to changes in the local atomic structure in the liquid phase [21]. These effects control the creation of the short-range atomic configuration. Changes in the short-range ordering are manifested as dumping rearrangements of atoms in the long-range ordering, leading to stabilization of the supercooled liquid state (long-range order would be necessary for progress into the crystallization process) [20].

4. Conclusions

The XRD and Mössbauer investigations confirm that the described production method, in which molten alloy is injected into a copper die, facilitates the manufacture of rod-shaped bulk amorphous alloy samples corresponding to the formula: $Fe_{61}Co_{10}Ti_{3-x}Y_{6+x}B_{20}$ (x = 0, 1). The crystallization process is a complex and in the investigated alloys occurs in one or two stages. DSC curve for $Fe_{61}Co_{10}Ti_3Y_6B_{20}$ alloy shows near situated peaks, whereas the crystallization process for $Fe_{61}Co_{10}Ti_2Y_7B_{20}$ alloy takes place in one stage.

On the basis of the performed investigations it can be stated that the $Fe_{61}Co_{10}Ti_2Y_7B_{20}$ is a material more homogeneous and characterized by a greater packing density of atoms (larger value B_{hf} and D_{sp}). Additionally, it has more value saturation magnetization and lower coercivity field.

REFERENCES

[1] P. Duwez, R.H. Willens, T. Metall. Soc. Aime. **227**, 362–365 (1963).
[2] M. Nabiałek, J. Zbroszczyk, J. Olszewski, M. Hasiak, W. Ciurzyńska, K. Sobczyk, J. Świerczek, J. Kaleta, A. Łukiewska, J. Magn. Magn. Mater. **324**, 787-791 (2008).
[3] J. Garus, S. Garus, M. Nabiałek, M. Szota, Acta Phys.Pol. A **126**, 954-956 (2014).
[4] J. Gondro, K. Błoch, M. Nabiałek, K. Waltters, M. Szota, Arch. Metall. Mater. **60**, 1071-1074 (2015).
[5] M. Dospial, J. Olszewski, M. Nabialek, P. Pietrusiewicz, T. Kaczmarzyk, Nukleonika **60**, 15-18 (2015).
[6] M. Nabiałek., P. Pietrusiewicz, M. Szota, M. Dośpiał, J. Jędryka, K. Szota, S. Lesz, Arch. Metall. Mater. **57**, 223-227 (2012).
[7] J. Gondro, J. Świerczek, J. Olszewski, J. Zbroszczyk, K. Sobczyk, W. Ciurzyńska, J. Rzącki, M. Nabiałek, J. Magn. Magn. Mater. **324**, 1360-1364 (2012).
[8] K. Błoch, J. Magn. Magn. Mater. **390**, 118-122 (2015).
[9] J. Gondro, J. Świerczek, K. Błoch, J. Zbroszczyk, W. Ciurzyńska, J. Olszewski, Physica B. **445**, 37-41 (2014).
[10] S. Lesz, R. Babilas, M. Nabialek, M. Szota, M. Dospial, R. Nowosielski, J. All. Compd. **509**, 197-201 (2010).
[11] W.H. Wang, C. Dong, C.H. Shek, Mater. Sci. Eng. **44**, 45–89 (2004).
[12] H.W. Chang, Y.C. Huang, C.W. Chang, C.H. Chiu, W.C. Chang, J. All. Compd. **462**, 68-72 (2008).
[13] H. Kronmüller, J. Appl. Phys. **52 (3)**, 1859 – 1864 (1981).
[14] H. Kronmüller, IEEE Trans. Magn., MAG-15, **5**, 1218-1225 (1979).
[15] N. Lenge, H. Kronmüller, Phys. Stat. Sol. (a), **95**, 621-633 (1986).
[16] P. Pietrusiewicz, M. Nabiałek, M. Dośpiał, K. Gruszka, K. Błoch, J. Gondro, P. Brągiel, M. Szota, Z. Stradomski, J. All. Compd. 615, Suppt 1, **5**, S67–S70 (2014).
[17] K. Gruszka, M. Nabiałek, K. Błoch S. Walters, Int. J. Mater. Res. **106**, 689-696 (2015).
[18] Z. P. Lu, C. T. Liu, J. Mat. Sci. **39**, 3965-3974 (2004).
[19] K. Gruszka, M. Nabiałek, K. Błoch, J. Olszewski, Nukleonika

60, No.1, 23-27 (2015).

[20] M. Nabiałek., J. Alloys and Compd. **642**, 98-103 (2015).

[21] Z. Long, Y. Shao, F. Xu, H. Wei, Z. Zhang, P. Zhang, X. Su, Mater. Sci. Eng. **164**, 1-5 (2009).

Received: 20 March 2015.